ACS central science

Open Access

http://pubs.acs.org/journal/acscii

Article

Flipping the GPCR Switch: Structure-Based Development of Selective Cannabinoid Receptor 2 Inverse Agonists

Miroslav Kosar, Roman C. Sarott, David A. Sykes, Alexander E. G. Viray, Rosa Maria Vitale, Nataša Tomašević, Xiaoting Li, Rudolf L. Z. Ganzoni, Bilal Kicin, Lisa Reichert, Kacper J. Patej, Uxía Gómez-Bouzó, Wolfgang Guba, Peter J. McCormick, Tian Hua, Christian W. Gruber, Dmitry B. Veprintsev, James A. Frank,* Uwe Grether,* and Erick M. Carreira*

Cite This: *ACS Cent. Sci.* 2024, 10, 956−968

Read Online

ACCESS | Metrics & More | Article Recommendations | Supporting Information

ABSTRACT: We report a blueprint for the rational design of G protein coupled receptor (GPCR) ligands with a tailored functional response. The present study discloses the structure-based design of cannabinoid receptor type 2 (CB_2R) selective inverse agonists (*S*)-**1** and (*R*)-**1**, which were derived from privileged agonist HU-308 by introduction of a phenyl group at the *gem*-dimethylheptyl side chain. Epimer (*R*)-**1** exhibits high affinity for CB_2R with K_d = 39.1 nM and serves as a platform for the synthesis of a wide variety of probes. Notably, for the first time these fluorescent probes retain their inverse agonist functionality, high affinity, and selectivity for CB_2R independent of linker and fluorophore substitution. Ligands (*S*)-**1**, (*R*)-**1**, and their derivatives act as inverse agonists in CB_2R-mediated cAMP as well as G protein recruitment assays and do not trigger *β*-arrestin−receptor association. Furthermore, no receptor activation was detected in live cell $ERK_{1/2}$ phosphorylation and Ca^{2+}-release assays. Confocal fluorescence imaging experiments with (*R*)-**7** (Alexa488) and (*R*)-**9** (Alexa647) probes employing BV-2 microglial cells visualized CB_2R expressed at endogenous levels. Finally, molecular dynamics simulations corroborate the initial docking data in which inverse agonists restrict movement of toggle switch $Trp258^{6.48}$ and thereby stabilize CB_2R in its inactive state.

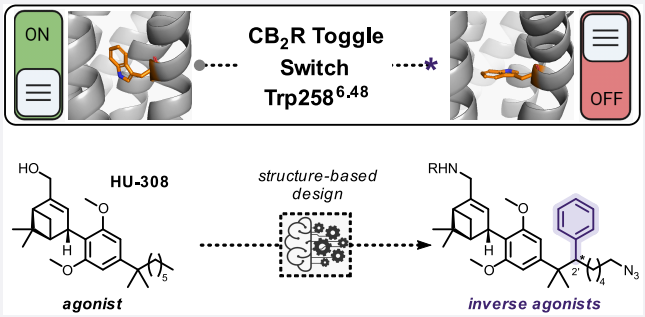

INTRODUCTION

The endocannabinoid system is present in all vertebrates and comprises endogenous ligands, enzymes mediating ligand metabolism, transporters, and the two prominent cannabinoid receptors type 1 and type 2 (CB_1R and CB_2R).[1,2] Exploitation of the therapeutic potential of CB_2R has primarily focused on receptor activation with agonists and showed promise to ameliorate a plethora of diseases, such as autoimmune[3] and metabolic disorders,[4,5] chronic pain,[6] and multiple sclerosis.[7] By contrast, CB_2R antagonists and inverse agonists remain vastly underexplored despite encouraging results in models of arthritis[8] and neuroinflammation.[9−11] Notably, CB_2R antagonist TT-816 is currently being investigated in a phase II clinical trial as an immune checkpoint inhibitor for the treatment of solid tumors.[12]

Despite the current considerable endeavors to deliver selective CB_2R therapeutics,[12−19] to date there are no such drugs available on the market. Poor understanding of CB_2R localization, expression, and signaling on the molecular level are key factors responsible for this absence.[20] Elucidation of CB_2R pharmacology has been hampered by the insufficient specificity of monoclonal antibodies[21−24] and the scarcity of reliable chemical probes.[25] Although some potent, selective, and validated fluorescent probes have been reported,[26−28] these function as agonists that disturb cellular homeostasis by triggering downstream signaling and *β*-arrestin association, followed by agonist-mediated receptor internalization.[29,30] These limitations may be addressed by implementation of inverse agonist based fluoroprobes that do not prompt receptor endocytosis. Additionally, inverse agonists tend to possess greater affinity for receptors in the more populous inactive G protein coupled receptor (GPCR) conformation yielding improved specificity and signal-to-noise ratio of probes compared to agonists.[31]

Historically, development of high-affinity, selective fluorescent CB_2R inverse agonists has proven arduous. In the cases reported, fluorophore conjugation completely ablated[32] or materially reduced[33] affinity. In one example, a study of a series

Received: November 28, 2023
Revised: February 20, 2024
Accepted: February 20, 2024
Published: March 11, 2024

Scheme 1. Novel Structure-Based Design of HU-308-Derived CB_2R-Selective Inverse Agonists That Actuate $Trp258^{6.48}$ Toggle Switch

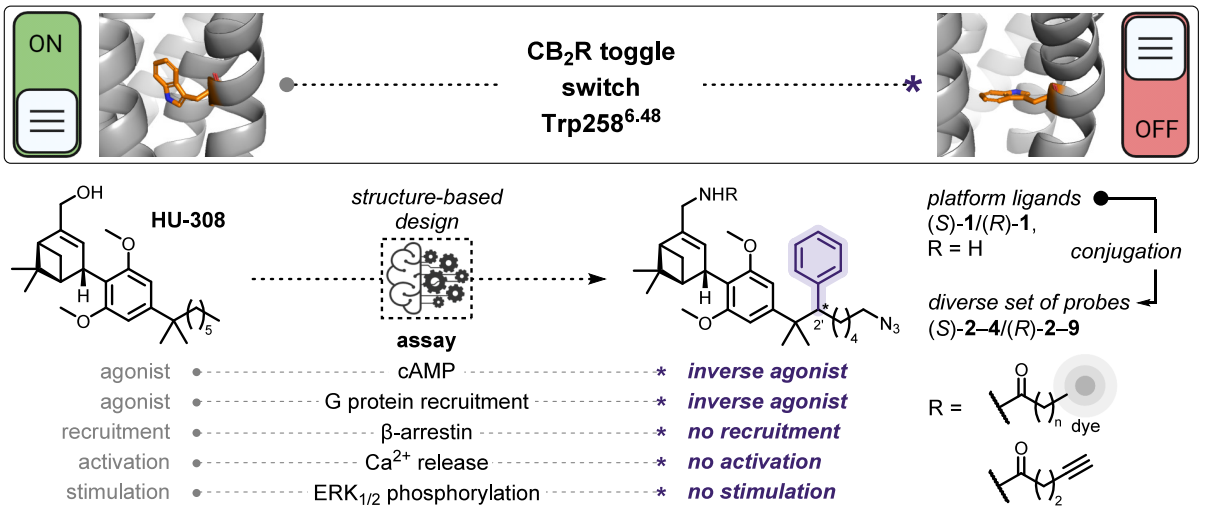

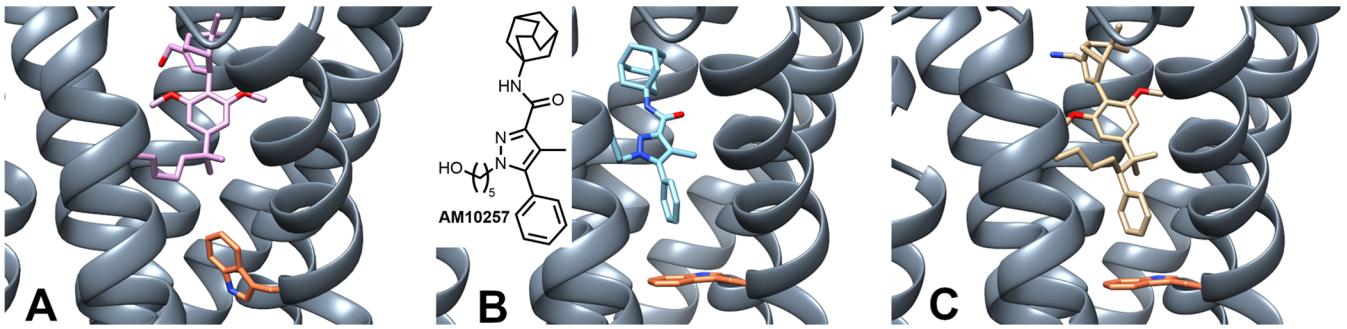

Figure 1. Comparison of active (A, PDB 8GUS, ligand HU-308)[48] and inactive (B, PDB 5ZTY, ligand AM10257)[49] CB_2R conformations. (C) Docking study of HU-308-derived putative inverse agonist (*R*)-**1** in the inactive CB_2R conformation (PDB 5ZTY). (*R*)-**1** reaches into the secondary pocket occupied by the toggle switch responsible for CB_2R activation, $Trp258^{6.48}$ (orange), and shares binding interactions virtually identical with those of AM10257.

of agonists led to the identification of a specific linker–fluorophore construct endowing inverse agonism in a cAMP assay.[34] Development of a potent, selective, and versatile CB_2R-targeting inverse agonist scaffold that can be conjugated to a variety of fluorophores and functionalities remains an unmet challenge.

Since its discovery in 1999,[35] CB_2R-selective agonist HU-308 (Scheme 1) has enjoyed privileged status for the study of CB_2R pharmacology.[36] HU-308 has been extensively applied to unravel effects of CB_2R activation in animal models of pain,[37] osteoporosis,[38] Parkinson's disease,[39] and amyotrophic lateral sclerosis[40] and is currently investigated in phase I clinical trials for mitigation of inflammation.[19] The pharmacophore embedded in HU-308 has served in the development of photoswitchable,[41] fluorescent,[28,42] and ligand-directed covalent probes.[26] On the basis of our prior work with HU-308, we focused on this scaffold with the intent of transforming its functional profile from agonist to inverse agonist with minimal structural modification. In this respect, Schapira and Jones have independently discussed the conceptual benefits of working with a set of molecules closely related in structure to enable in-depth understanding of receptor pharmacology.[43,44]

The past two decades witnessed the exponential rise of reported GPCR structures; hence, structure-based ligand design is at present ideally positioned to capitalize on the ongoing revolution.[45] Since more than a third of all approved drugs exert their action by GPCR modulation, it is vital to comprehensively investigate and understand receptor pharmacology with functionally orthogonal chemical probes.[46] GPCRs of the most populous class A family are distinguished by high homology of the CWxP motif. In particular, the toggle switch of CWxP that modulates receptor activation, $Trp258^{6.48}$, is conserved within 78% of nonolfactory GPCRs.[47] Examination of the X-ray structure of CB_2R in its inactive conformation revealed a secondary binding pocket that hosts $Trp258^{6.48}$. Further investigation by in silico docking suggested that addition of a substituent at C(2′) of HU-308 might constrain $Trp258^{6.48}$ and hence modulate CB_2R activation (Scheme 1).

We report novel inverse agonists that demonstrate avid binding at CB_2R with excellent selectivity over the closely related CB_1R. The compounds were profiled for their functional response in a comprehensive panel of in vitro (*β*-arrestin and G protein recruitment) as well as cellular (cAMP, $ERK_{1/2}$ phosphorylation, Ca^{2+} signaling) assays. Remarkably, none of the probes activate CB_2R-mediated signaling in any of the tested pathways. Fluorescent probes demonstrated excellent specificity and visualized CB_2R expressed at endogenous levels in live-cell confocal microscopy experiments. Finally, molecular dynamics simulations investigated

https://doi.org/10.1021/acscentsci.3c01461
ACS Cent. Sci. 2024, 10, 956−968

structural determinants that prevent receptor activation upon ligand binding and corroborate movement restriction of Trp258$^{6.48}$. The workflow and key considerations described herein may be used to successfully drive future structure-based switch of functionality involving ligands and proteins beyond HU-308 and CB_2R.

RESULTS AND DISCUSSION

In Silico Probe Design. We have investigated the recently published active (PDB 8GUS, Figure 1A)[48] and inactive (PDB 5ZTY, Figure 1B)[49] conformations of CB_2R crystallized with agonist HU-308 and antagonist/inverse agonist AM10257, respectively. Close examination of the two receptor conformations revealed that AM10257 reaches into a secondary binding pocket that features a highly conserved CWxP motif in class A GPCRs[50] and moreover hosts Trp258$^{6.48}$, the recently designated single residue toggle switch of CB_2R activation.[51]

Comparison of the two receptor conformations combined with in silico docking suggested that a phenyl substituent introduced α to the *gem*-dimethyl group of HU-308 might occupy the same lipophilic subpocket as the phenyl of AM10257. The phenyl substitution creates a new C(2′) stereocenter at the pendent side chain; accordingly the explicit (*S*) and (*R*) designations preceding compound labels denote its absolute configuration. Additionally, structural features were incorporated that proved critical in our prior works to bestow excellent pharmacological profiles, yielding ligands (*S*)-**1** and (*R*)-**1** (Figure 2).[26,28,42] Namely, terminal azide was inserted and the allylic alcohol was substituted by an amine to allow facile, stable conjugation to fluorophores and confer improved affinity and selectivity for CB_2R. The novel putative HU-308-derived inverse agonist (*R*)-**1** showed binding interactions virtually identical with those of AM10257 in the inactive CB_2R conformation (Figure 1C). In particular, the C(2′) phenyl group of (*R*)-**1** oriented toward Trp258$^{6.48}$ and attained a favorable edge-to-face π-interaction similar to the phenyl of AM10257. The nearly identical interactions are essential as we have hypothesized that the impediment of the upward movement of Trp258$^{6.48}$ may effectively prevent receptor activation.

Synthesis. Access to (*S*)-**1** and (*R*)-**1** that feature a phenyl group at the homobenzylic position of cannabinoid scaffolds α to a sterically demanding *gem*-dimethyl group is synthetically challenging and unprecedented. Prior structure−activity relationship studies on cannabinoid ligands focused almost exclusively on the easily accessible benzylic or ω-position of the pendent side chain.[52] To the best of our knowledge, there is only a single report of substitution at the homobenzylic position with a methyl group in a structure of Δ^8-THC that lacks the sterically congesting *gem*-dimethyl motif.[53]

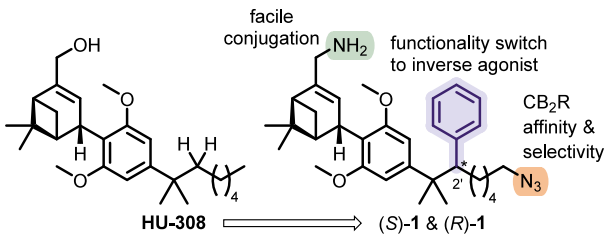

Figure 2. Design of inverse agonists (*S*)-**1** and (*R*)-**1**.

The synthesis of (*S*)-**1**/(*R*)-**1** commenced with **10**, which was prepared by methylation of 3,5-dimethoxyphenylacetonitrile and subsequent treatment with phenyl lithium (Scheme 2).[54,55] Introduction of the alkyl side chain to ketone **10** proved a formidable challenge due to steric hindrance. Initial attempts using established phosphonium ylide routes yielded no reaction even at elevated temperatures.[56,57] An extensive screening of Grignard reagents either yielded no reaction or afforded exclusively Grignard reduction product **11**. Finally, using a modified procedure for the preparation of alkyl lithiums by Punzalan,[58] we employed, for the first time, 5-chloropentyl lithium to forge the tertiary alcohol **12** in 83% yield.[59] Subsequent Chugaev elimination of the benzylic alcohol under mild conditions yielded **13** in 95% yield. BBr_3-mediated demethylation followed by high-pressure hydrogenation over Pd/C afforded (*S*)-**14**/(*R*)-**14** as a racemic mixture in 94% yield over two steps. The synthesis was continued with the racemate to rapidly access material for initial pharmacological evaluation. To this end, Friedel−Crafts allylation with verbenol derivative **15** followed by treatment with $(MeO)_2SO_2$ furnished methylated epimeric mixture (*S*)-**16**/(*R*)-**16** in 50% yield over the two steps. Subsequent substitution of the primary alkyl chloride with NaN_3 and hydrazine-mediated phthalimide deprotection revealed allylic amines (*S*)-**1**/(*R*)-**1** in 73% yield. Finally, the synthesis was concluded by functionalization of the diastereomeric mixture (*S*)-**1**/(*R*)-**1** with DY-480XL or 4-pentynoic acid to yield mixtures of epimers (*S*)-**2**/(*R*)-**2** and (*S*)-**3**/(*R*)-**3**, respectively.

We then investigated access to epimers (*S*)-**1** and (*R*)-**1** separately. Following introduction of verbenol fragment **15**, screening of conditions to separate the resulting epimers ((*S*)-**16**/(*R*)-**16**) by silica gel chromatography, HPLC, and supercritical fluid chromatography (SFC) proved unsuccessful. Gratifyingly, we found that enantiomers (*S*)-**14**/(*R*)-**14** could be separated by semipreparative SFC using a chiral stationary phase to yield (*S*)-**14** and (*R*)-**14** in >99% ee and 96% ee, respectively. Resorcinols (*S*)-**14** and (*R*)-**14** were then functionalized to yield enantio- and diastereomerically pure (*S*)-**1**−(*S*)-**4** and (*R*)-**1**−(*R*)-**9**. To assign the absolute configuration at the C(2′) stereocenter, (*S*)-**14** was converted to a *p*-nitrobenzoate (*S*)-**17**, whose structure was elucidated by X-ray crystallography.

Pharmacological Profiling. *Saturation Binding Assays.* We assessed whether the phenyl substitution in (*S*)-**1**, (*R*)-**1**, and their derivatives (*S*)-**2**−(*S*)-**4** and (*R*)-**2**−(*R*)-**9** impedes interaction with CB_2R. To this end, time-resolved Förster resonance energy transfer (TR-FRET) binding assay was employed to determine the affinities of the new probes at room temperature.[28] HEK293 membrane preparations of SNAP-Lumi4-Tb labeled hCB_2R were incubated with a fluorescent probe in the presence or absence of a validated inverse agonist, SR-144,528,[36] to determine its binding parameters. Gratifyingly, the epimeric mixture (*S*)-**2**/(*R*)-**2** demonstrated good affinity for CB_2R (K_d = 67.9 nM), suggesting that the C(2′) functionalization was well tolerated and validated the in silico guided design.

Encouraged by the promising result, we studied the impact of configuration at the C(2′) stereocenter on the pharmacological properties by examining each epimer individually. A 12-fold greater binding affinity for CB_2R was shown by (*R*)-**1** (K_d = 39.1 nM) in comparison to (*S*)-**1** (K_d = 476 nM). Functionalization of (*S*)-**1** and (*R*)-**1** with 4-pentynoic acid

https://doi.org/10.1021/acscentsci.3c01461
ACS Cent. Sci. 2024, 10, 956−968

Scheme 2. Synthesis of Novel CB_2R-Selective HU-308-Derived Inverse Agonists[a]

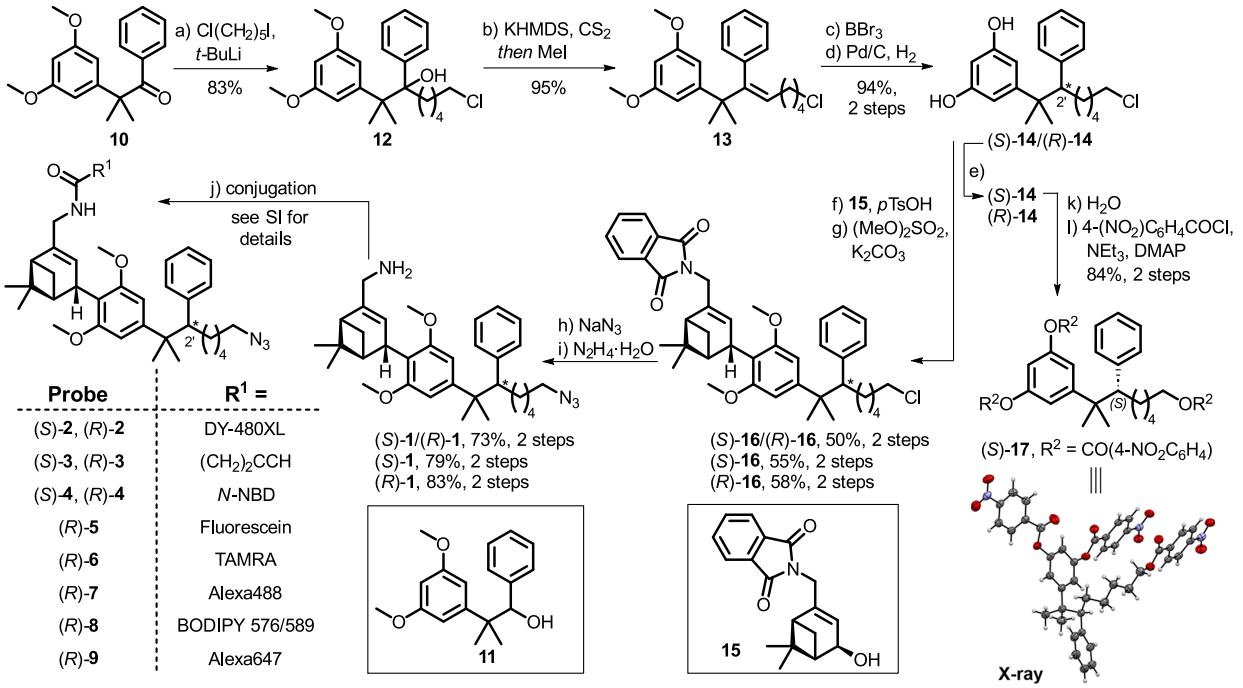

[a]Reagents and conditions: (a) 1-chloro-5-iodopentane, *t*-BuLi, *n*-pentane, Et_2O, −78 °C to rt, 83%; (b) KHMDS, CS_2, THF, −78 °C to rt and then MeI, 40 °C, 95%; (c) BBr_3, CH_2Cl_2, 0 °C, 97%; (d) Pd/C, H_2, EtOAc, rt, 97%; (e) semipreparative SFC, (*S*)-**14**, 25%, >99% ee, (*R*)-**14**, 20%, 96% ee; (f) **15**, *p*TsOH·H_2O, CH_2Cl_2, rt, 64−71%; (g) $(MeO)_2SO_2$, K_2CO_3, acetone, rt, 78−82%; (h) NaN_3, DMF, 50 °C, 88−96%; (i) N_2H_4·H_2O, (*E*)/(*Z*)-crotyl alcohol, EtOH, 75 °C, 76−94%; (j) for conjugation conditions and details, see Supporting Information; (k) H_2O, microwave irradiation, 150 °C, 99%; (l) 4-nitrobenzoyl chloride, NEt_3, DMAP, CH_2Cl_2, rt, 85%.

was well tolerated, and the resulting compounds, (*S*)-**3** and (*R*)-**3**, retained the stereoisomeric preference with K_d = 2.10 and 0.42 nM, respectively. Conjugation of (*S*)-**1** and (*R*)-**1** with DY-480XL and *N*-NBD yielded probes (*S*)-**2** and (*R*)-**2** and (*S*)-**4** and (*R*)-**4**, respectively. Fluoroprobes (*S*)-**2** and (*S*)-**4** displayed inferior CB_2R affinity (K_d = 162 and 158 nM, respectively) compared to the excellent binding potencies of (*R*)-**2** and (*R*)-**4** (K_d = 10.2 and 12.3 nM, respectively). Furthermore, strong agreement was observed between CB_2R K_d and K_i values obtained by independent TR-FRET and radioligand binding assays for (*R*)-**2** (K_d = 10.2 nM and K_i = 8.26 nM) and (*R*)-**3** (K_d = 0.42 nM and K_i = 0.66 nM). Collectively, the results further validate the TR-FRET assay and imply that the orthosteric binding pocket of CB_2R shows preference for the *R*-epimer of the parent compound and its derivatives.

We then set out to investigate whether the excellent CB_2R affinities of (*R*)-**1**−(*R*)-**4** are impacted by linker and fluorophore substitution. To this end, probes (*R*)-**5**−(*R*)-**9** were prepared that feature a variety of linker lengths and fluorophores, spanning a wide range of size, lipophilicity, and membrane permeability. When tested by TR-FRET at 37 °C, fluorescein, tetramethylrhodamine (TAMRA), and Alexa488 bearing probes (*R*)-**5**, (*R*)-**6**, and (*R*)-**7** all emerged as high affinity binders for CB_2R with excellent K_d values of 30.3, 2.78, and 24.9 nM, respectively (Table 1). BODIPY 576/589 conjugate (*R*)-**8** showed good binding potency with CB_2R, K_d = 44.7 nM. Particularly remarkable was the retention of high affinity displayed by probe (*R*)-**9** (K_d = 25.9 nM) functionalized with Alexa647. These results illustrate substantial improvement over previous work with agonists where functionalization with the highly polar Alexa488 and sterically demanding Alexa647 led to 64-fold and 611-fold drops in affinity, respectively.[28] Importantly, fluoroprobes (*R*)-**5**, (*R*)-**6**, (*R*)-**7**, and (*R*)-**9** emit robust fluorescence signals with exquisite specific binding windows when tested at the physiologically relevant temperature, 37 °C (see Figure 3 and Figure S1).

Table 1. TR-FRET-Based Profiling of Binding Affinity[a]

		K_d [nM]		
probe	dye	CB_2R	CB_1R	K_d ratio (CB_1R/CB_2R)
(*R*)-**2**	DY-480XL	18.9	1740	92
(*R*)-**5**	fluorescein	30.3	1280	42
(*R*)-**6**	TAMRA	2.78	396	142
(*R*)-**7**	Alexa488	24.9	3300	133
(*R*)-**9**	Alexa647	25.9	7050	272

[a]Saturation binding data (K_d) were determined in a TR-FRET assay at 37 °C with membrane preparations from either hCB_2R-HEK293 or hCB_1R-HEK293 cells. Data shown as a mean, N = 3.

The binding selectivity of fluorescent probes was tested against the closely related CB_1R in a saturation binding assay at 37 °C using membrane preparations derived from HEK293 cells expressing hCB_1R (Table 1). Fluoroprobes (*R*)-**2**, (*R*)-**5**, (*R*)-**6**, and (*R*)-**7** displayed 42−142-fold selectivity for CB_2R over CB_1R. Notably, (*R*)-**9** demonstrated an exceptional 272-fold preference for CB_2R over CB_1R. Collectively, the excellent affinity and selectivity of a range of physicochemically distinct substituents and fluorophores highlight the versatility of novel platform ligand (*R*)-**1**.

Kinetic Binding TR-FRET Assay. We were intrigued by the performances of our probes in the saturation binding assay and leveraged TR-FRET to study ligand binding kinetics at a

https://doi.org/10.1021/acscentsci.3c01461
ACS Cent. Sci. 2024, 10, 956−968

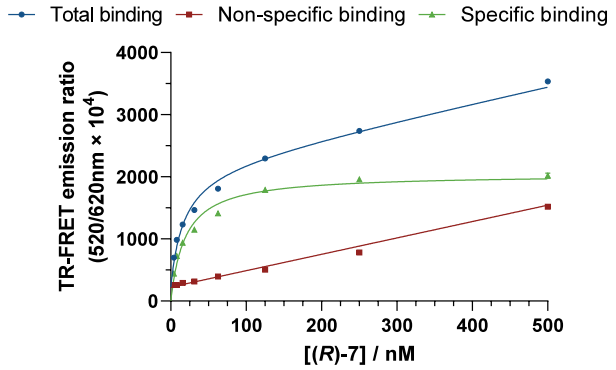

Figure 3. TR-FRET-based saturation binding profile of (*R*)-**7** (Alexa488) at CB_2R determined at 37 °C. Nonspecific binding was determined in the presence of SR-144,528 (10 μM). Data shown as a mean ± SEM, $N = 3$.

physiologically relevant temperature, 37 °C (Table 2). The results suggest that all compounds, except (*S*)-**1**, possess dramatically slower receptor dissociation rates, k_{off}, in comparison to the control inverse agonist, SR-144,528. Therefore, high CB_2R affinity of the probes once bound stems from slow receptor dissociation rates. The probes are thus endowed with long receptor residence times, τ, an attribute that has been argued particularly important for GPCRs[60] as a better suited determinant, compared to K_d, of ligand−protein interactions in living systems.[61,62] Importantly, excellent agreement was found between K_d values obtained in saturation and kinetic binding experiments.

Functional Profiling: cAMP, G Protein Recruitment, and β-Arrestin. HU-308 is a potent full agonist at CB_2R in the [^{35}S]-GTPγS assay, triggers inhibition of cAMP production, promotes recruitment of β-arrestin, stimulates $ERK_{1/2}$ phosphorylation, and facilitates release of Ca^{2+} from intracellular stores.[36,41,63] Compounding evidence indicates that distinct CB_2R agonists favor discrete receptor conformations, leading to preferential activation of one specific signaling pathway over another, a phenomenon known as biased agonism.[36,64−66] Accordingly, we have dedicated substantial efforts to comprehensively profile the pharmacological responses elicited by the new probes across known CB_2R signaling pathways.

One of the canonical signaling pathways of CB_2R involves association with $G\alpha_{i/o}$ proteins, which elicit reversible inhibition of adenylyl cyclase resulting in a decrease of cellular cAMP levels and suppression of protein kinase A activity.[67]

Table 2. TR-FRET-Based Kinetic Profiling at CB_2R[a]

probe	k_{on} [10^6 M^{-1} min^{-1}]	k_{off} [10^{-2} min^{-1}]	τ [min]	kinetic K_d [nM]
(*S*)-**1**	9.39	115	0.87	122
(*R*)-**1**	12.0	13.9	7.19	11.6
(*S*)-**3**	44.3	4.96	20.2	1.12
(*R*)-**3**	88.7	2.29	43.7	0.26
(*R*)-**6**	3.60	1.08	92.6	3.00
(*R*)-**7**	1.49	2.37	42.2	15.9
(*R*)-**9**	1.75	1.71	58.5	9.77
SR-144,528	240	122	0.82	5.08

[a]Kinetic K_d data were measured at 37 °C in a TR-FRET assay using hCB_2R-HEK293 membrane preparations. Data shown as a mean, $N = 3$.

Consequently, we have investigated the change in cAMP levels upon probe addition using homogeneous time-resolved fluorescence (HTRF) cAMP assay (Table 3).

All compounds behaved as inverse agonists, with efficacy (E_{max}) ranging between −31 and −55%. Both epimers of the parent amine ligand inhibited cAMP production with the (*R*)-**1** stereoisomer demonstrating greater potency ($pEC_{50} = 6.95$) than (*S*)-**1** ($pEC_{50} = 5.57$). DY-480XL and alkyne functionalized probes, (*R*)-**2** ($pEC_{50} = 7.15$) and (*R*)-**3** ($pEC_{50} = 7.48$), were favored over (*S*)-**2** ($pEC_{50} = 6.47$) and (*S*)-**3** ($pEC_{50} = 7.39$) with respect to potency, albeit to a lesser degree. Interestingly, the *N*-NBD probes (*S*)-**4** and (*R*)-**4** behaved as inverse agonists only at high concentration ($pEC_{50} = 4.98$ and 5.91, respectively). As a control, we prepared HU-308-derived agonist probe **ago-3** from **ago-1** that features the same scaffold as (*S*)-**3** and (*R*)-**3** except that it lacks the C(2′) phenyl substituent (eq 1). In the cAMP assay **ago-3** displayed potent receptor activation ($pEC_{50} = 8.47$, $E_{max} = 112\%$). These results provide direct experimental evidence as to the critical role of the phenyl substituent in facilitating the switch in ligand functionality from agonist to inverse agonist.

To complement the functional response elicited in the cAMP assay, we tested whether the probes trigger association of $G\alpha_i$ protein with CB_2R using our recently reported bioluminescence resonance energy transfer (BRET) Gi-CASE assay.[68] Membrane preparations harvested from hCB_2R-HEK293 T-REx cells that genetically incorporate fluorescent NanoLuciferase donor and Venus acceptor proteins to the Gα and Gγ subunits, respectively, were incubated with a probe, and the change in BRET signal was detected. Agonist binding triggers CB_2R activation and dissociation of the Gα and G$\beta\gamma$ subunits resulting in BRET signal reduction. Conversely, inverse agonists elicit increase in BRET intensity by stabilization of inactive CB_2R conformation and G protein accumulation beyond the basal level. Compounds (*S*)-**1**, (*R*)-**1**, (*S*)-**3**, and (*R*)-**3** were selected as representatives to circumvent interference among fluorophores in the BRET assay as previously reported.[34] The results indicate that all tested compounds behave as potent inverse agonists with respect to G protein recruitment at CB_2R (Figure 4 and Table 4).

Alkyne functionalized probes (*S*)-**3** and (*R*)-**3** ($pEC_{50} = 7.51$ and 7.22, respectively) have shown superior potency in comparison to free amines (*S*)-**1** and (*R*)-**1** ($pEC_{50} = 6.72$ and 6.80, respectively). Control agonist HU-210 and inverse

Table 3. Functional Characterization in a CB_2R cAMP Assay[a]

probe	pEC_{50}	E_{max} [%]
(*S*)-**1**	5.57	−44
(*R*)-**1**	6.95	−44
(*S*)-**2**	6.47	−37
(*R*)-**2**	7.15	−31
(*S*)-**3**	7.39	−49
(*R*)-**3**	7.48	−55
(*S*)-**4**[b]	4.98	+44
(*R*)-**4**	5.91	−40
ago-3	8.47	+112

[a]Potency (pEC_{50}) and E_{max} data were obtained in a cAMP HTRF assay using hCB_2R-CHO cells. Data were normalized to agonist CP-55,940 response (100%) and basal level (0%), unless noted otherwise. [b]Data were normalized to the response of inverse agonist AM10257 (0%) and basal level (100%). Data shown as a mean, $N = 3$.

https://doi.org/10.1021/acscentsci.3c01461
ACS Cent. Sci. 2024, 10, 956−968

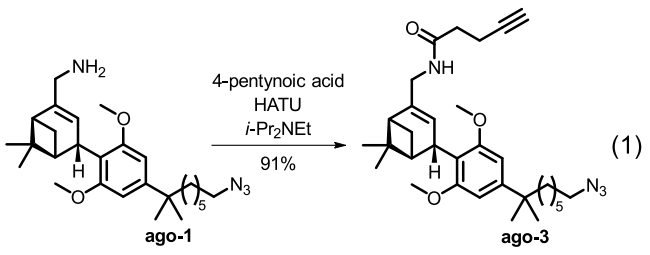

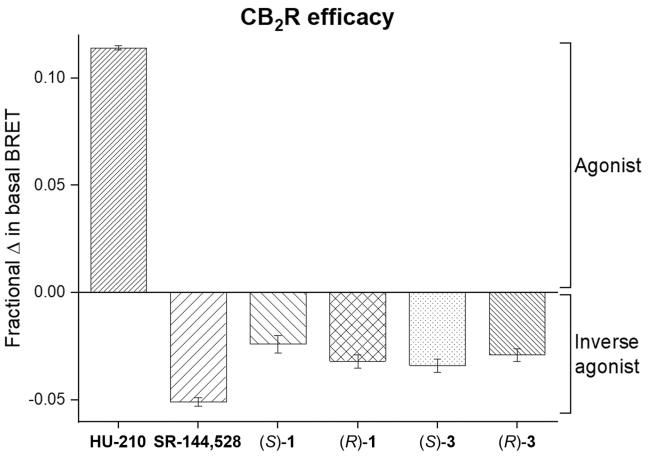

Figure 4. BRET-based Gi-CASE membrane assay to characterize G protein recruitment at CB_2R. Efficacy, E_{max}, of the compounds is shown as a mean ± SEM, N = 3−4.

Table 4. Functional Characterization of G Protein Recruitment at CB_2R in a BRET Gi-CASE Assay[a]

probe	pEC_{50}	E_{max} [%]
(*S*)-**1**	6.72	−21
(*R*)-**1**	6.80	−28
(*S*)-**3**	7.51	−30
(*R*)-**3**	7.22	−25
SR-144,528	8.23	−45

[a]Potency (pEC_{50}) and E_{max} data were obtained in a Gi-CASE BRET-based assay using membrane preparations from hCB_2R-HEK293 T-REx cells. Data were normalized to agonist HU-210 response (100%) and basal level (0%). Data are shown as mean, N = 3−4.

agonist SR-144,528 demonstrated potency consistent with previously reported [^{35}S]-GTPγS binding assay values, further validating the experimental results (pEC_{50} = 8.83 and 8.23, respectively).[36,69] With respect to efficacy (E_{max}), probes (*S*)-**1**, (*R*)-**1**, (*S*)-**3**, and (*R*)-**3** induced functional responses between −21 and −30%. Remarkably, comparison of the effects elicited by (*S*)-**1** in the cAMP and Gi-CASE assays (pEC_{50} = 5.57 and 6.72, respectively) suggests 14-fold increased potency of G protein recruitment over adenylyl cyclase inhibition, a striking bias within a CB_2R−$G\alpha_i$-mediated pathway.

Among the best studied G protein independent signaling pathways of CB_2R is the β-arrestin cascade. β-Arrestins bind activated CB_2R following receptor phosphorylation, block further G protein mediated signaling, and destine the receptor for internalization.[30] Representative compounds were profiled for β-arrestin recruitment in a BRET assay where an increase of the BRET ratio corresponds to recruitment of β-arrestin. Baseline BRET signal was retained by (*S*)-**1**, (*R*)-**1**, (*S*)-**3**, and (*R*)-**3** (Figure 5). In contrast, control agonists HU-308 and HU-210 showed expected recruitment of β-arrestin to CB_2R as

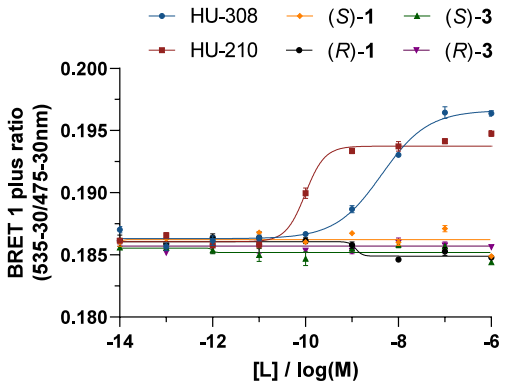

Figure 5. BRET-based assay to characterize β-arrestin recruitment at CB_2R. L = ligand. Data are a representative of N = 3.

indicated by increases in BRET intensity (pEC_{50} = 8.37 and 10.0, respectively). These results imply that (*S*)-**1**, (*R*)-**1**, (*S*)-**3**, and (*R*)-**3** do not activate CB_2R toward β-arrestin recruitment.

Phosphorylation of ERK. Activation of CB_2R is associated with downstream stimulation of mitogen-activated protein kinases, such as $ERK_{1/2}$, mediated via either Gβγ or β-arrestins.[70,71] We have tested representative high-affinity fluorescent probe (*R*)-**2** for CB_2R-mediated phosphorylation of endogenous $ERK_{1/2}$ in a CB_2R inducible breast cancer HCC1954 cell line using the AlphaScreen SureFire phospho-ERK assay (Figure 6). Expression of CB_2R was optionally induced with doxycycline (DOX), and after 24 h the cells were incubated with a vehicle (0.1% DMSO), CB_2R selective agonist JWH133[72] (1 μM), or (*R*)-**2** (1 μM) for 30 min. Following cell lysis, lysates were incubated with a mixture containing donor and acceptor beads for 2 h at room temperature and the luminescence emission signal was measured.

In the absence of CB_2R expression inducer (DOX), the phosphorylation levels of $ERK_{1/2}$ remained the same for cells treated with a vehicle, agonist JWH133, and (*R*)-**2**. In cells induced to express CB_2R with DOX (1 μg/mL), JWH133

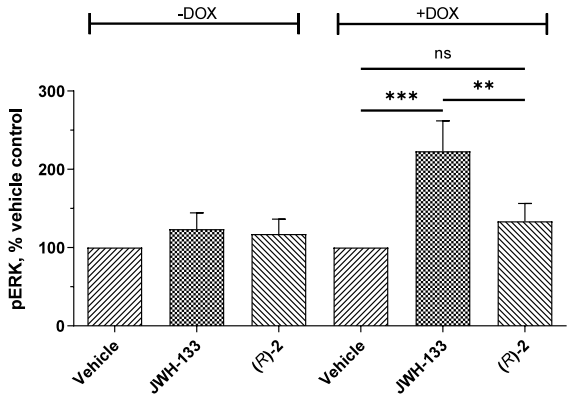

Figure 6. Live cell AlphaScreen SureFire phospho-ERK assay with CB_2R inducible breast cancer HCC1954 cell line. Cells were optionally induced with doxycycline (DOX) for 24 h to stimulate expression of CB_2R followed by incubation with a vehicle (0.1% DMSO), agonist JWH133[72] (1 μM), or (*R*)-**2** (1 μM) for 30 min. Statistical significance was examined by one-way ANOVA followed by Tukey's *post hoc* test. ns = nonsignificant, **, $p < 0.01$; ***, $p < 0.001$. Data are an average of three independent biological replicates.

https://doi.org/10.1021/acscentsci.3c01461
ACS Cent. Sci. 2024, 10, 956−968

effectively stimulated $ERK_{1/2}$ phosphorylation mediated by CB_2R activation, in agreement with previously reported findings.[73] Addition of (*R*)-**2** had no effect on the level of phosphorylated $ERK_{1/2}$, which remained the same as for a vehicle. Data of the phospho-ERK cellular assay imply that (*R*)-**2** does not induce phosphorylation of $ERK_{1/2}$ by either CB_2R-mediated G$\beta\gamma$ or β-arrestin signaling (or by non-CB_2R-mediated pathways).

Ca^{2+} Signaling. Upon activation of CB_2R, Ca^{2+} is often released from intracellular reservoirs.[74−76] Our previous work reported that HU-308 and its photoswitchable derivative, *azo*-HU-308, increase intracellular Ca^{2+} in the mouse AtT-20 cell line.[41] Naturally, we were intrigued to investigate the response elicited by our probes. The epimeric mixture (*S*)-**3**/(*R*)-**3** was chosen to avoid fluorophore interference with the Fluo-4AM Ca^{2+} dye and test both diastereomers simultaneously.

Live AtT-20 cells overexpressing rat CB_2R [AtT-20(rCB_2R)] were treated with Fluo-4AM Ca^{2+} dye and imaged by confocal microscopy (Figure 7). Addition of (*S*)-**3**/(*R*)-**3** (20 μM) did not elicit increase in Fluo-4AM fluorescence, whereas subsequent addition of agonist HU-308 (20 μM) triggered a robust fluorescence spike. Ionomycin was added at the end of the experiment to saturate Ca^{2+} levels. This result indicates that neither (*S*)-**3** nor (*R*)-**3** induces Ca^{2+} release via CB_2R activation and suggests that the probes can be displaced by HU-308.

Fluorescence Confocal Microscopy in Live Cells. Having validated that the probes do not trigger CB_2R signaling at multiple downstream pathways, we employed (*R*)-**7** and (*R*)-**9** to visualize CB_2R by confocal fluorescence microscopy. Probes (*R*)-**7** and (*R*)-**9** were selected due to their bright, photostable, and extensively applied fluorophores Alexa488 and Alexa647. Additionally, the green- and red-shifted fluorescence spectra of (*R*)-**7** and (*R*)-**9** provide flexibility and potential for synergy with additional fluorescent proteins and small molecule dyes for multiplexed imaging studies.

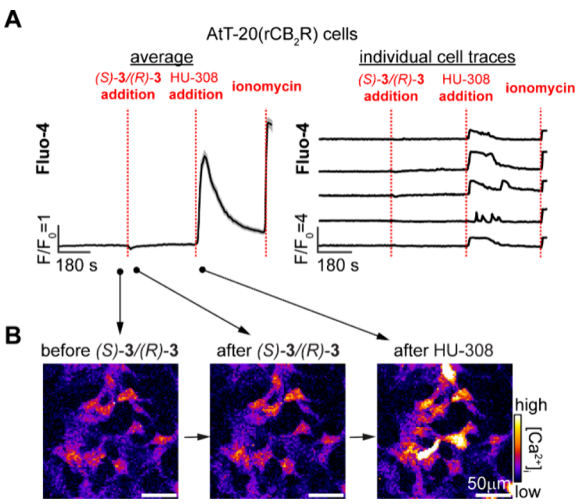

Figure 7. Live cell fluorescent Ca^{2+} imaging in rat CB_2R overexpressing AtT-20 cells [AtT-20(rCB_2R)] loaded with Fluo-4AM (2 μM). After initial equilibration, (*S*)-**3**/(*R*)-**3** (20 μM) was added, followed by HU-308 (20 μM) and ionomycin (10 μM). Shown are the average responses of 200 cells (A, left), individual traces of five representative cells (A, right), and representative fluorescence images from different time points (B). Averaged data plotted as mean ± SEM, T = 4.

First, AtT-20 cells stably expressing *N*-terminal SNAP-tagged human CB_2R [AtT-20(SNAP-hCB_2R)] were coincubated with (*R*)-**7**, Janelia Fluor SNAP-549i (JF549i), and Hoechst33342 to label CB_2R, SNAP-tags, and nuclei, respectively. Confocal microscopy revealed bright fluorescence of Alexa488 and JF549i delineating the plasma membranes of AtT-20 cells (Figure 8A). Analysis of the corresponding intensity plot showed virtually identical colocalization overlap between the Alexa488 ((*R*)-**7**) and JF549i (SNAP-hCB_2R) signals (Figure 8A).

Since many cannabinoid ligands tend to accumulate in plasma membranes due to their lipophilic nature, specificity of (*R*)-**7** and (*R*)-**9** for CB_2R was evaluated using AtT-20(rCB_2R) and AtT-20 wild-type (WT) cells, which do not express CB_2R.[77] AtT-20(rCB_2R) and AtT-20(WT) cells were incubated with (*R*)-**7** and Hoechst33342 and imaged by confocal microscopy. A robust Alexa488 fluorescence signal was detected at the plasma membrane of AtT-20(rCB_2R) cells (Figure 8B, left). In stark contrast, AtT-20(WT) cells showed only minimal background fluorescence with no signal stemming from the cellular membrane (Figure 8B, right). These results confirm that (*R*)-**7** specifically labels CB_2R at the plasma membrane.

Encouraged by the promising results with (*R*)-**7** in cells overexpressing CB_2R, we proceeded to investigate the probes' ability to detect CB_2R at endogenous expression levels. To this end, the murine derived BV-2 microglial cell line was selected due to its extensive use as a high fidelity, primary microglia culture model[78] that was applied in the study of neurodegeneration and neuroinflammation.[79−81] Importantly, BV-2 cells endogenously express CB_2R.[82,83] Following incubation of BV-2 cells with (*R*)-**7** and Hoechst33342, an intense Alexa488 signal was observed at the plasma membrane across BV-2 cells (Figure 8C). These results confirm that (*R*)-**7** can visualize CB_2R at endogenous expression levels. Importantly, when (*R*)-**9** (Alexa647) was subjected to analogous experiments, it demonstrated equal specificity for CB_2R in AtT-20 cells (see Figure S2A,B) combined with strong signal intensity in the BV-2 microglial cell line (see Figure S2C). Finally, these data imply that the performances of (*R*)-**7** and (*R*)-**9** remain uncompromised by interspecies differences and the probes can be employed to investigate both human and murine orthologs of CB_2R.

Molecular Dynamics Simulations Unravel Pharmacophore Determinants of Receptor Activation. Molecular dynamics (MD) studies were performed in a membrane environment with inverse agonists (*S*)-**3** and (*R*)-**3** and their agonist counterpart **ago-3** to contrast their interactions with CB_2R at a molecular level and elucidate their orthogonal functional profiles. To this end, the X-ray structure of CB_2R in an inactive state in complex with AM10257 (PDB 5ZTY) was selected as a starting point for 1 μs MD simulations to assess ligand stability and identify rearrangements within the binding site.

All three ligands adopt an L-shape conformation with the pendent alkyl chain hosted in a cleft formed by $Phe183^{ECL2}$, $Tyr190^{5.39}$, $Trp194^{5.43}$, and $Thr114^{3.33}$ (see Figure 9 and Figures S3 and S4). The resorcinol engages in $\pi-\pi$ interactions with $Phe183^{ECL2}$, while the pinene core is surrounded by aromatic residues ($Phe183^{ECL2}$, $Phe91^{2.61}$, and $Phe94^{2.64}$). An rmsd plot of **ago-3** following a best fit of protein backbone shows an initial rearrangement followed by a periodic "breathinglike" motion of the resorcinol and alkyl chain that

https://doi.org/10.1021/acscentsci.3c01461
ACS Cent. Sci. 2024, 10, 956−968

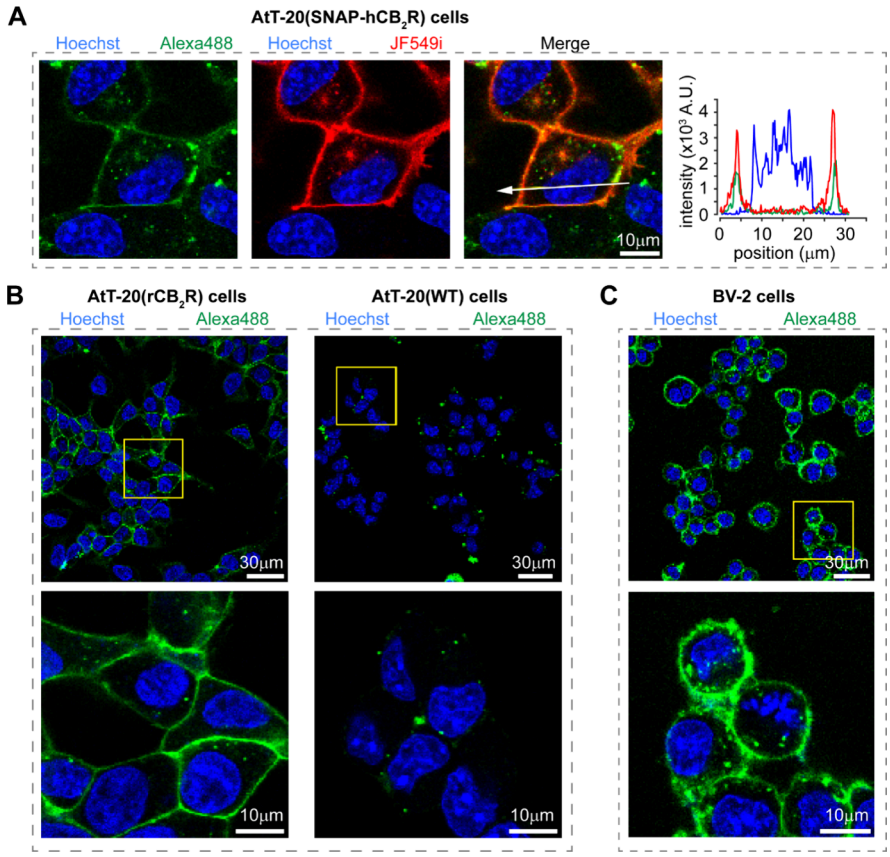

Figure 8. Confocal imaging of (*R*)-**7** in live cell lines. (A) AtT-20(SNAP-hCB$_2$R) cells were labeled for 15 min with (*R*)-**7** (Alexa488, 625 nM, green), SNAP-JF549i (JF549i, 500 nM, red), and Hoechst33342 (Hoechst, 1 μM, blue) to visualize CB$_2$R, SNAP-tags, and nuclei, respectively. Fluorescence intensity profiles across the white line for Alexa488, JF549i, and Hoechst33342 are shown on the right. (B) AtT-20(rCB$_2$R) cells (left) and AtT-20(WT) cells (right) were treated with (*R*)-**7** (625 nM, green) and Hoechst33342 (1 μM, blue) for 15 min and imaged by confocal microscopy. (C) Live BV-2 microglial cells that endogenously express CB$_2$R were incubated with (*R*)-**7** (2.5 μM, green) and Hoechst33342 (1 μM, blue) for 15 min and imaged by confocal microscopy.

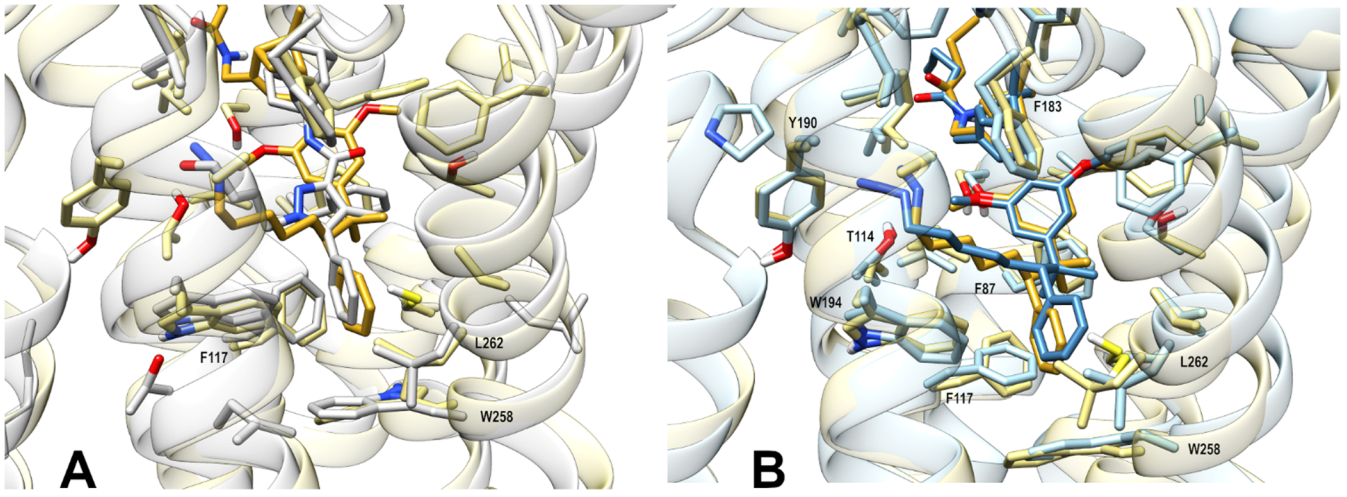

Figure 9. Representative frames from molecular dynamics (MD) simulations of CB$_2$R (PDB 5ZTY) in complex with (*S*)-**3** or (*R*)-**3**. Superimposition at level of protein backbone of (A) CB$_2$R X-ray structure with AM10257 (light gray) and (*R*)-**3** MD complex (ligand in gold and protein in light yellow) and of (B) the two inverse agonist complexes (*S*)-**3** (ligand in blue and protein light blue) and (*R*)-**3** (ligand in gold and protein in light yellow).

oscillates between bent and flat conformations (see Figures S3 and S5). Furthermore, in accord with our earlier work,[42] in the CB$_2$R–**ago-3** complex the amide group of **ago-3** forms a stable hydrogen bond with the carbonyl of Ser90$^{2.60}$.

In agreement with the in silico docking (Figure 1), the MD simulations suggest the C(2′) phenyl rings of (*S*)-**3** and (*R*)-**3** mirror that of AM10257 and engage in $\pi-\pi$ contacts with Phe117$^{3.36}$ and Trp258$^{6.48}$ (see Figure 9A and Figure S6). In contrast to **ago-3**, no initial rearrangement in the binding poses

https://doi.org/10.1021/acscentsci.3c01461
ACS Cent. Sci. 2024, 10, 956−968

of (*S*)-**3** and (*R*)-**3** was observed in their rmsd plots (see Figure S7). Ligands (*S*)-**3** and (*R*)-**3** share similar binding modes of the pinene-resorcinol core; however, significant differences are observed in the orientation adopted by *gem*-dimethyl groups and the C(2′) phenyl rings (see Figure 9B and Figure S8). In particular, the *gem*-dimethyl group of (*S*)-**3** is rotated clockwise compared to that of (*R*)-**3** and the C(2′) phenyl of (*S*)-**3** is rotated toward Leu262$^{6.44}$, inducing a minor displacement of helix H6, while that of (*R*)-**3** protrudes deeper toward Trp258$^{6.48}$. In both cases, the conformation of the Trp258$^{6.48}$ toggle switch is restricted and CB_2R is thus stabilized in its inactive state, in stark contrast to the interactions observed with the agonist complex.

Superimposition of CB_2R protein backbone employing the X-ray structure with AM10257 and the representative MD frames in complex with either (*S*)-**3** (see Figure S6) or (*R*)-**3** (Figure 9A) imply that (*R*)-**3** more closely resembles the binding mode of AM10257 in the crystallized complex. In particular, the secondary binding pocket featuring Trp258$^{6.48}$ and the surrounding residues Phe117$^{3.36}$ and Leu262$^{6.44}$ are in excellent agreement between AM10257 and (*R*)-**3**.

Finally, the difference in free energy of binding ($\Delta\Delta G$) was determined for (*R*)-**3** and (*S*)-**3** using molecular mechanics/Poisson−Boltzmann (generalized Born) surface area (MM/PB(GB)SA) calculations (see Table S1). The data imply that binding of (*R*)-**3** is more stable by −0.76 kcal mol^{-1} (MM/GBSA) and −0.40 kcal mol^{-1} (MM/PBSA) in comparison to (*S*)-**3**. Notably, the calculated $\Delta\Delta G$ values are in agreement with the experimental difference of $\Delta\Delta G$ = −0.9 kcal mol^{-1} for epimers (*S*)-**3** and (*R*)-**3**.

CONCLUSION

This study describes the in silico guided, structure-based switch of functionality from agonist to inverse agonist of HU-308, a ligand extensively applied to unravel CB_2R pharmacology and currently investigated in clinical trials. The novel inverse agonist platform ligands (*S*)-**1** and (*R*)-**1** demonstrated high binding affinity for CB_2R and selectivity against CB_1R that was retained upon functionalization with a range of chemically distinct substituents and fluorophores. The functional response exerted on CB_2R by (*S*)-**1**, (*R*)-**1**, and their derivatives was evaluated by HTRF and BRET and implied an inverse agonist profile in cAMP as well as G protein recruitment assays, and no induction of β-arrestin−receptor association. Live cell experiments with (*R*)-**2** and (*S*)-**3**/(*R*)-**3** demonstrated that the probes do not activate CB_2R toward $ERK_{1/2}$ phosphorylation and Ca^{2+} signaling pathways, respectively. Fluorescence microscopy experiments with (*R*)-**7** and (*R*)-**9** in AtT-20 cells expressing human and rat CB_2R isoforms demonstrated excellent target specificity and species translatability. Treatment of the BV-2 microglial cell line with (*R*)-**7** and (*R*)-**9** allowed imaging of endogenous CB_2R in live cells. Finally, MD simulations with (*S*)-**3**, (*R*)-**3**, and **ago-3** corroborate the critical role of the C(2′) phenyl substituent in conferring the functional profile by modulating the CB_2R toggle switch Trp258$^{6.48}$ of the CWxP motif.

More broadly, this work discloses the first ligand platform for CB_2R that retains its inverse agonist functional profile, affinity, and selectivity independent of its conjugation to a range of diverse functional groups. The probes introduce a long-sought-after complementarity to an agonist-dominated toolkit to study, elucidate and unlock the full therapeutic potential of CB_2R. Moreover, the platform ligands promise broad application and synergy with previously published work which awaited discovery of an inverse agonist.[26] The exponential rise in resolved structures of class A GPCRs, many of which are available in inactive, intermediate, and fully active states, has enabled unprecedented insight into the mechanism of receptor activation.[50,84,85] Thus, the strategy and experimental framework disclosed herein may aid in the structure-based design of agonists, antagonists, and inverse agonists for GPCRs beyond CB_2R.

ASSOCIATED CONTENT

Supporting Information

The Supporting Information is available free of charge at https://pubs.acs.org/doi/10.1021/acscentsci.3c01461.

Experimental procedures and characterization data for all compounds (PDF)

AUTHOR INFORMATION

Corresponding Authors

James A. Frank − *Department of Chemical Physiology & Biochemistry, Oregon Health & Science University, Portland, Oregon 97239-3098, United States; Vollum Institute, Oregon Health & Science University, Portland, Oregon 97239-3098, United States;* orcid.org/0000-0001-6705-2540; Email: frankja@ohsu.edu

Uwe Grether − *Roche Pharma Research & Early Development, Roche Innovation Center Basel, F. Hoffmann-La Roche Ltd., 4070 Basel, Switzerland;* orcid.org/0000-0002-3164-9270; Email: uwe.grether@roche.com

Erick M. Carreira − *Laboratorium für Organische Chemie, Eidgenössische Technische Hochschule Zürich, 8093 Zürich, Switzerland;* orcid.org/0000-0003-1472-490X; Email: erickm.carreira@org.chem.ethz.ch

Authors

Miroslav Kosar − *Laboratorium für Organische Chemie, Eidgenössische Technische Hochschule Zürich, 8093 Zürich, Switzerland;* orcid.org/0000-0003-0166-7571

Roman C. Sarott − *Laboratorium für Organische Chemie, Eidgenössische Technische Hochschule Zürich, 8093 Zürich, Switzerland;* orcid.org/0000-0001-8789-6150

David A. Sykes − *Faculty of Medicine & Health Sciences, University of Nottingham, Nottingham NG7 2UH, U.K.; Centre of Membrane Proteins and Receptors (COMPARE), University of Birmingham and University of Nottingham,* https://www.birmingham-nottingham.ac.uk/compare

Alexander E. G. Viray − *Department of Chemical Physiology & Biochemistry, Oregon Health & Science University, Portland, Oregon 97239-3098, United States*

Rosa Maria Vitale − *Institute of Biomolecular Chemistry, National Research Council, 80078 Pozzuoli, Italy;* orcid.org/0000-0001-9243-1307

Nataša Tomašević − *Center for Physiology and Pharmacology, Medical University of Vienna, 1090 Vienna, Austria*

Xiaoting Li − *iHuman Institute, ShanghaiTech University, Shanghai 201210, China*

Rudolf L. Z. Ganzoni − *Laboratorium für Organische Chemie, Eidgenössische Technische Hochschule Zürich, 8093 Zürich, Switzerland*

Bilal Kicin − *Laboratorium für Organische Chemie, Eidgenössische Technische Hochschule Zürich, 8093 Zürich, Switzerland;* orcid.org/0009-0001-7676-7115

https://doi.org/10.1021/acscentsci.3c01461
ACS Cent. Sci. 2024, 10, 956−968

Lisa Reichert − *Laboratorium für Organische Chemie, Eidgenössische Technische Hochschule Zürich, 8093 Zürich, Switzerland*

Kacper J. Patej − *Laboratorium für Organische Chemie, Eidgenössische Technische Hochschule Zürich, 8093 Zürich, Switzerland*

Uxía Gómez-Bouzó − *Laboratorium für Organische Chemie, Eidgenössische Technische Hochschule Zürich, 8093 Zürich, Switzerland*

Wolfgang Guba − *Roche Pharma Research & Early Development, Roche Innovation Center Basel, F. Hoffmann-La Roche Ltd., 4070 Basel, Switzerland;* orcid.org/0000-0002-3285-5957

Peter J. McCormick − *Department of Pharmacology and Therapeutics, University of Liverpool, Liverpool L69 3GE, U.K.*

Tian Hua − *iHuman Institute, ShanghaiTech University, Shanghai 201210, China*

Christian W. Gruber − *Center for Physiology and Pharmacology, Medical University of Vienna, 1090 Vienna, Austria;* orcid.org/0000-0001-6060-7048

Dmitry B. Veprintsev − *Faculty of Medicine & Health Sciences, University of Nottingham, Nottingham NG7 2UH, U.K.; Centre of Membrane Proteins and Receptors (COMPARE), University of Birmingham and University of Nottingham,* https://www.birmingham-nottingham.ac.uk/compare; orcid.org/0000-0002-3583-5409

Complete contact information is available at: https://pubs.acs.org/10.1021/acscentsci.3c01461

Notes

The authors declare the following competing financial interest(s): M.K., R.C.S., B.K., W.G., U.G., and E.M.C. have filed a patent on CB2R selective modulators and fluorescent probes.

■ ACKNOWLEDGMENTS

We thank Eric Bald for his help with chiral separations and Isabelle Kaufmann for her assistance with logistics and administration. We are grateful to Raphael Bigler, Paolo Tosatti, Stephan Bachmann, Kurt Püntener, and Manuela Müller for their expertise, insight, and experimental help with high-pressure hydrogenations. We thank René Arnold, Rainer Frankenstein, and Stephan Burkhardt for their help with NMR measurements, Jan Kovacovic for his expertise with high-pressure hydrogenation, and the MoBiAS team for MS analysis. We are grateful to Nils Trapp and Michael Solar for X-ray crystallographic analysis. M.K. and R.C.S. gratefully acknowledge a fellowship by the Scholarship Fund of the Swiss Chemical Industry (SSCI). MD studies have been funded by project code PIR01_00011 "IBISCo", PON 2014-2020. We would like to thank Jürg Gertsch (University of Bern, Switzerland) for kindly providing the CB_2R expressing cells. Research in the laboratory of C.W.G. has been supported by the Austrian Science Fund (FWF) through project P32109. N.T. has been supported by a short-term scientific mission (STSM) grant from the EU COST Action CA 18133 (ERNEST). B.K. gratefully acknowledges the SNF fund 200020_188538. T.H. has been supported by the National Key Research and Development Program of China grant 2022YFA1302903. D.A.S. and D.B.V. gratefully acknowledge funding by Roche postdoctoral fellowship RPF-551.

■ REFERENCES

(1) Maccarrone, M.; Di Marzo, V.; Gertsch, J.; Grether, U.; Howlett, A. C.; Hua, T.; Makriyannis, A.; Piomelli, D.; Ueda, N.; van der Stelt, M. Goods and Bads of the Endocannabinoid System as a Therapeutic Target: Lessons Learned after 30 Years. *Pharmacol. Rev.* **2023**, *75*, 885−958.

(2) Munro, S.; Thomas, K. L.; Abu-Shaar, M. Molecular characterization of a peripheral receptor for cannabinoids. *Nature* **1993**, *365*, 61−65.

(3) Goncalves, E. D.; Dutra, R. C. Cannabinoid receptors as therapeutic targets for autoimmune diseases: where do we stand? *Drug Discovery Today* **2019**, *24*, 1845−1853.

(4) Rossi, F.; Punzo, F.; Umano, G. R.; Argenziano, M.; Miraglia Del Giudice, E. Role of Cannabinoids in Obesity. *Int. J. Mol. Sci.* **2018**, *19*, 2690−2700.

(5) Kumawat, V. S.; Kaur, G. Therapeutic potential of cannabinoid receptor 2 in the treatment of diabetes mellitus and its complications. *Eur. J. Pharmacol.* **2019**, *862*, 172628−172633.

(6) Shang, Y.; Tang, Y. The central cannabinoid receptor type-2 (CB2) and chronic pain. *Int. J. Neurosci.* **2017**, *127*, 812−823.

(7) Khan, H.; Ghori, F. K.; Ghani, U.; Javed, A.; Zahid, S. Cannabinoid and endocannabinoid system: a promising therapeutic intervention for multiple sclerosis. *Mol. Biol. Rep.* **2022**, *49*, 5117−5131.

(8) Lunn, C. A.; Reich, E. P.; Fine, J. S.; Lavey, B.; Kozlowski, J. A.; Hipkin, R. W.; Lundell, D. J.; Bober, L. Biology and therapeutic potential of cannabinoid CB2 receptor inverse agonists. *Br. J. Pharmacol.* **2008**, *153*, 226−239.

(9) Reiner, A.; Heldt, S. A.; Presley, C. S.; Guley, N. H.; Elberger, A. J.; Deng, Y.; D'Surney, L.; Rogers, J. T.; Ferrell, J.; Bu, W.; Del Mar, N.; Honig, M. G.; Gurley, S. N.; Moore, B. M., II Motor, visual and emotional deficits in mice after closed-head mild traumatic brain injury are alleviated by the novel CB2 inverse agonist SMM-189. *Int. J. Mol. Sci.* **2015**, *16*, 758−787.

(10) Bu, W.; Ren, H.; Deng, Y.; Del Mar, N.; Guley, N. M.; Moore, B. M.; Honig, M. G.; Reiner, A. Mild Traumatic Brain Injury Produces Neuron Loss That Can Be Rescued by Modulating Microglial Activation Using a CB2 Receptor Inverse Agonist. *Front. Neurosci.* **2016**, *10*, 449.

(11) Alghamdi, S. S.; Mustafa, S. M.; Moore, B. M., II Synthesis and biological evaluation of a ring analogs of the selective CB2 inverse agonist SMM-189. *Bioorg. Med. Chem. Lett.* **2021**, *33*, 116035.

(12) *TT-816 as Monotherapy or in Combination With a PD-1 Inhibitor in Patients With Advanced Cancers (SEABEAM) (MK3475-E88)*. ClincialTrials.gov. https://clinicaltrials.gov/study/NCT05525455 (accessed 2023-11-07).

(13) *A Study to Investigate the Efficacy and Safety of RG7774 in Patients With Diabetes Mellitus Type 1 or Type 2 With Treatment-Naive Diabetic Retinopathy (CANBERRA)*. ClincialTrials.gov. https://www.clinicaltrials.gov/study/NCT04265261 (accessed 2023-09-19).

(14) *NTRX-07*. NeuroTherapia. https://www.neurotherapia.com/research (accessed 2024-01-04).

(15) *Safety and Tolerability of NTRX-07 in Healthy Volunteers*. ClincialTrials.gov. https://www.clinicaltrials.gov/study/NCT04375436 (accessed 2024-01-04).

(16) *CNTX-6016*. Centrexion. https://centrexion.com/science/pipeline/ (accessed 2024-01-04).

(17) *Safety, Tolerability & Pharmacokinetics Study of CNTX-6016 in Healthy Subjects and Subjects With PDN*. ClincialTrials.gov. https://clinicaltrials.gov/study/NCT04857957 (accessed 2024-01-04).

(18) *Olorinab - Pfizer*. AdisInsight.https://adisinsight.springer.com/drugs/800039670 (accessed 2024-01-04).

(19) *ARDS003*. Tetra Bio-Pharma. https://tetrabiopharma.com/pipeline/ (accessed 2023-09-19).

(20) Whiting, Z. M.; Yin, J.; de la Harpe, S. M.; Vernall, A. J.; Grimsey, N. L. Developing the Cannabinoid Receptor 2 (CB2) pharmacopoeia: past, present, and future. *Trends Pharmacol. Sci.* **2022**, *43*, 754−771.

(21) Brownjohn, P. W.; Ashton, J. C. Spinal cannabinoid CB2 receptors as a target for neuropathic pain: an investigation using chronic constriction injury. *Neuroscience* **2012**, *203*, 180−193.
(22) Cecyre, B.; Thomas, S.; Ptito, M.; Casanova, C.; Bouchard, J. F. Evaluation of the specificity of antibodies raised against cannabinoid receptor type 2 in the mouse retina. *Naunyn-Schmiedebergs Arch. Pharmacol.* **2014**, *387*, 175−184.
(23) Marchalant, Y.; Brownjohn, P. W.; Bonnet, A.; Kleffmann, T.; Ashton, J. C. Validating Antibodies to the Cannabinoid CB2 Receptor: Antibody Sensitivity Is Not Evidence of Antibody Specificity. *J. Histochem. Cytochem.* **2014**, *62*, 395−404.
(24) Zhang, H. Y.; Shen, H.; Jordan, C. J.; Liu, Q. R.; Gardner, E. L.; Bonci, A.; Xi, Z. X. CB2 receptor antibody signal specificity: correlations with the use of partial CB2-knockout mice and anti-rat CB2 receptor antibodies. *Acta Pharmacol. Sin.* **2019**, *40*, 398−409.
(25) Chen, D. J.; Gao, M.; Gao, F. F.; Su, Q. X.; Wu, J. Brain cannabinoid receptor 2: expression, function and modulation. *Acta Pharmacol. Sin.* **2017**, *38*, 312−316.
(26) Kosar, M.; Sykes, D. A.; Viray, A. E. G.; Vitale, R. M.; Sarott, R. C.; Ganzoni, R. L.; Onion, D.; Tobias, J. M.; Leippe, P.; Ullmer, C.; Zirwes, E. A.; Guba, W.; Grether, U.; Frank, J. A.; Veprintsev, D. B.; Carreira, E. M. Platform Reagents Enable Synthesis of Ligand-Directed Covalent Probes: Study of Cannabinoid Receptor 2 in Live Cells. *J. Am. Chem. Soc.* **2023**, *145*, 15094−15108.
(27) Gazzi, T.; Brennecke, B.; Atz, K.; Korn, C.; Sykes, D.; Forn-Cuni, G.; Pfaff, P.; Sarott, R. C.; Westphal, M. V.; Mostinski, Y.; Mach, L.; Wasinska-Kalwa, M.; Weise, M.; Hoare, B. L.; Miljuš, T.; Mexi, M.; Roth, N.; Koers, E. J.; Guba, W.; Alker, A.; Rufer, A. C.; Kusznir, E. A.; Huber, S.; Raposo, C.; Zirwes, E. A.; Osterwald, A.; Pavlovic, A.; Moes, S.; Beck, J.; Nettekoven, M.; Benito-Cuesta, I.; Grande, T.; Drawnel, F.; Widmer, G.; Holzer, D.; van der Wel, T.; Mandhair, H.; Honer, M.; Fingerle, J.; Scheffel, J.; Broichhagen, J.; Gawrisch, K.; Romero, J.; Hillard, C. J.; Varga, Z. V.; van der Stelt, M.; Pacher, P.; Gertsch, J.; Ullmer, C.; McCormick, P. J.; Oddi, S.; Spaink, H. P.; Maccarrone, M.; Veprintsev, D. B.; Carreira, E. M.; Grether, U.; Nazaré, M. Detection of cannabinoid receptor type 2 in native cells and zebrafish with a highly potent, cell-permeable fluorescent probe. *Chem. Sci.* **2022**, *13*, 5539−5545.
(28) Sarott, R. C.; Westphal, M. V.; Pfaff, P.; Korn, C.; Sykes, D. A.; Gazzi, T.; Brennecke, B.; Atz, K.; Weise, M.; Mostinski, Y.; Hompluem, P.; Koers, E.; Miljus, T.; Roth, N. J.; Asmelash, H.; Vong, M. C.; Piovesan, J.; Guba, W.; Rufer, A. C.; Kusznir, E. A.; Huber, S.; Raposo, C.; Zirwes, E. A.; Osterwald, A.; Pavlovic, A.; Moes, S.; Beck, J.; Benito-Cuesta, I.; Grande, T.; Ruiz de Martin Esteban, S.; Yeliseev, A.; Drawnel, F.; Widmer, G.; Holzer, D.; van der Wel, T.; Mandhair, H.; Yuan, C. Y.; Drobyski, W. R.; Saroz, Y.; Grimsey, N.; Honer, M.; Fingerle, J.; Gawrisch, K.; Romero, J.; Hillard, C. J.; Varga, Z. V.; van der Stelt, M.; Pacher, P.; Gertsch, J.; McCormick, P. J.; Ullmer, C.; Oddi, S.; Maccarrone, M.; Veprintsev, D. B.; Nazare, M.; Grether, U.; Carreira, E. M. Development of High-Specificity Fluorescent Probes to Enable Cannabinoid Type 2 Receptor Studies in Living Cells. *J. Am. Chem. Soc.* **2020**, *142*, 16953−16964.
(29) Grimsey, N. L.; Goodfellow, C. E.; Dragunow, M.; Glass, M. Cannabinoid receptor 2 undergoes Rab5-mediated internalization and recycles via a Rab11-dependent pathway. *Biochim. Biophys. Acta* **2011**, *1813*, 1554−1560.
(30) Chen, X.; Zheng, C.; Qian, J.; Sutton, S. W.; Wang, Z.; Lv, J.; Liu, C.; Zhou, N. Involvement of beta-arrestin-2 and clathrin in agonist-mediated internalization of the human cannabinoid CB2 receptor. *Curr. Mol. Pharmacol.* **2015**, *7*, 67−80.
(31) Weis, W. I.; Kobilka, B. K. The Molecular Basis of G Protein-Coupled Receptor Activation. *Annu. Rev. Biochem.* **2018**, *87*, 897−919.
(32) Cooper, A. G.; MacDonald, C.; Glass, M.; Hook, S.; Tyndall, J. D. A.; Vernall, A. J. Alkyl indole-based cannabinoid type 2 receptor tools: Exploration of linker and fluorophore attachment. *Eur. J. Med. Chem.* **2018**, *145*, 770−789.
(33) Sexton, M.; Woodruff, G.; Horne, E. A.; Lin, Y. H.; Muccioli, G. G.; Bai, M.; Stern, E.; Bornhop, D. J.; Stella, N. NIR-mbc94, a fluorescent ligand that binds to endogenous CB(2) receptors and is amenable to high-throughput screening. *Chem. Biol.* **2011**, *18*, 563−8.
(34) Singh, S.; Oyagawa, C. R. M.; Macdonald, C.; Grimsey, N. L.; Glass, M.; Vernall, A. J. Chromenopyrazole-based High Affinity, Selective Fluorescent Ligands for Cannabinoid Type 2 Receptor. *ACS Med. Chem. Lett.* **2019**, *10*, 209−214.
(35) Hanus, L.; Tchilibon, S.; Shiloah, S.; Goldenberg, D.; Horowitz, M.; Pertwee, R. G.; Ross, R. A.; Mechoulam, R.; Breuer, A.; Fride, E. Fride HU-308: A specific agonist for CB2, a peripheral cannabinoid receptor. *Proc. Natl. Acad. Sci. U. S. A.* **1999**, *96*, 14228−14233.
(36) Soethoudt, M.; Grether, U.; Fingerle, J.; Grim, T. W.; Fezza, F.; de Petrocellis, L.; Ullmer, C.; Rothenhausler, B.; Perret, C.; van Gils, N.; Finlay, D.; MacDonald, C.; Chicca, A.; Gens, M. D.; Stuart, J.; de Vries, H.; Mastrangelo, N.; Xia, L.; Alachouzos, G.; Baggelaar, M. P.; Martella, A.; Mock, E. D.; Deng, H.; Heitman, L. H.; Connor, M.; Di Marzo, V.; Gertsch, J.; Lichtman, A. H.; Maccarrone, M.; Pacher, P.; Glass, M.; van der Stelt, M. Cannabinoid CB2 receptor ligand profiling reveals biased signalling and off-target activity. *Nat. Commun.* **2017**, *8*, 13958.
(37) LaBuda, C. J.; Koblish, M.; Little, P. J. Cannabinoid CB2 receptor agonist activity in the hindpaw incision model of post-operative pain. *Eur. J. Pharmacol.* **2005**, *527*, 172−174.
(38) Ossola, C. A.; Surkin, P. N.; Mohn, C. E.; Elverdin, J. C.; Fernandez-Solari, J. Anti-Inflammatory and Osteoprotective Effects of Cannabinoid-2 Receptor Agonist HU-308 in a Rat Model of Lipopolysaccharide-Induced Periodontitis. *J. Periodontol.* **2016**, *87*, 725−734.
(39) Rentsch, P.; Stayte, S.; Egan, T.; Clark, I.; Vissel, B. Targeting the cannabinoid receptor CB2 in a mouse model of l-dopa induced dyskinesia. *Neurobiol. Dis.* **2020**, *134*, 104646−104659.
(40) Espejo-Porras, F.; Garcia-Toscano, L.; Rodriguez-Cueto, C.; Santos-Garcia, I.; de Lago, E.; Fernandez-Ruiz, J. Targeting glial cannabinoid CB(2) receptors to delay the progression of the pathological phenotype in TDP-43 (A315T) transgenic mice, a model of amyotrophic lateral sclerosis. *Br. J. Pharmacol.* **2019**, *176*, 1585−1600.
(41) Sarott, R. C.; Viray, A. E. G.; Pfaff, P.; Sadybekov, A.; Rajic, G.; Katritch, V.; Carreira, E. M.; Frank, J. A. Optical Control of Cannabinoid Receptor 2-Mediated Ca(2+) Release Enabled by Synthesis of Photoswitchable Probes. *J. Am. Chem. Soc.* **2021**, *143*, 736−743.
(42) Westphal, M. V.; Sarott, R. C.; Zirwes, E. A.; Osterwald, A.; Guba, W.; Ullmer, C.; Grether, U.; Carreira, E. M. Highly Selective, Amine-Derived Cannabinoid Receptor 2 Probes. *Chem.—Eur. J.* **2020**, *26*, 1380−1387.
(43) Lee, J.; Schapira, M. The Promise and Peril of Chemical Probe Negative Controls. *ACS Chem. Biol.* **2021**, *16*, 579−585.
(44) Bunnage, M. E.; Chekler, E. L.; Jones, L. H. Target validation using chemical probes. *Nat. Chem. Biol.* **2013**, *9*, 195−199.
(45) Congreve, M.; de Graaf, C.; Swain, N. A.; Tate, C. G. Impact of GPCR Structures on Drug Discovery. *Cell* **2020**, *181*, 81−91.
(46) Hauser, A. S.; Attwood, M. M.; Rask-Andersen, M.; Schioth, H. B.; Gloriam, D. E. Trends in GPCR drug discovery: new agents, targets and indications. *Nat. Rev. Drug Discovery* **2017**, *16*, 829−842.
(47) Olivella, M.; Caltabiano, G.; Cordomi, A. The role of Cysteine 6.47 in class A GPCRs. *BMC Struct. Biol.* **2013**, *13*, 3.
(48) Li, X.; Chang, H.; Bouma, J.; de Paus, L. V.; Mukhopadhyay, P.; Paloczi, J.; Mustafa, M.; van der Horst, C.; Kumar, S. S.; Wu, L.; Yu, Y.; van den Berg, R.; Janssen, A. P. A.; Lichtman, A.; Liu, Z. J.; Pacher, P.; van der Stelt, M.; Heitman, L. H.; Hua, T. Structural basis of selective cannabinoid CB(2) receptor activation. *Nat. Commun.* **2023**, *14*, 1447.
(49) Li, X.; Hua, T.; Vemuri, K.; Ho, J. H.; Wu, Y.; Wu, L.; Popov, P.; Benchama, O.; Zvonok, N.; Locke, K.; Qu, L.; Han, G. W.; Iyer, M. R.; Cinar, R.; Coffey, N. J.; Wang, J.; Wu, M.; Katritch, V.; Zhao, S.; Kunos, G.; Bohn, L. M.; Makriyannis, A.; Stevens, R. C.; Liu, Z. J.

https://doi.org/10.1021/acscentsci.3c01461
ACS Cent. Sci. 2024, 10, 956−968

Crystal Structure of the Human Cannabinoid Receptor CB2. *Cell* **2019**, *176*, 459−467.
(50) Zhou, Q.; Yang, D.; Wu, M.; Guo, Y.; Guo, W.; Zhong, L.; Cai, X.; Dai, A.; Jang, W.; Shakhnovich, E. I.; Liu, Z. J.; Stevens, R. C.; Lambert, N. A.; Babu, M. M.; Wang, M. W.; Zhao, S. Common activation mechanism of class A GPCRs. *eLife* **2019**, *8*, e50279.
(51) Hua, T.; Li, X.; Wu, L.; Iliopoulos-Tsoutsouvas, C.; Wang, Y.; Wu, M.; Shen, L.; Brust, C. A.; Nikas, S. P.; Song, F.; Song, X.; Yuan, S.; Sun, Q.; Wu, Y.; Jiang, S.; Grim, T. W.; Benchama, O.; Stahl, E. L.; Zvonok, N.; Zhao, S.; Bohn, L. M.; Makriyannis, A.; Liu, Z. J. Activation and Signaling Mechanism Revealed by Cannabinoid Receptor-Gi Complex Structures. *Cell* **2020**, *180*, 655−665.
(52) Bow, E. W.; Rimoldi, J. M. The Structure-Function Relationships of Classical Cannabinoids: CB1/CB2Modulation. *Perspect. Med. Chem.* **2016**, *8*, 17−39.
(53) Huffman, J. W.; Lainton, J. A. H.; Banner, W. K.; Duncan, S. G., Jr.; Jordan, R. D.; Yu, S.; Martin, B. R.; Wiley, J. L.; Compton, D. R.; Dai, D. Side chain methyl analogues of Δ8-THC. *Tetrahedron* **1997**, *53*, 1557−1576.
(54) Sharma, R.; Nikas, S. P.; Paronis, C. A.; Wood, J. T.; Halikhedkar, A.; Guo, J. J.; Thakur, G. A.; Kulkarni, S.; Benchama, O.; Raghav, J. G.; Gifford, R. S.; Jarbe, T. U.; Bergman, J.; Makriyannis, A. Controlled-deactivation cannabinergic ligands. *J. Med. Chem.* **2013**, *56*, 10142−10157.
(55) Corrie, J. E. T. Preparation and Properties of Unsymmetrical Benzoins and Related Compounds. *Tetrahedron* **1998**, *54*, 5407−5416.
(56) Zanato, C.; Pelagalli, A.; Marwick, K. F.; Piras, M.; Dall'Angelo, S.; Spinaci, A.; Pertwee, R. G.; Wyllie, D. J.; Hardingham, G. E.; Zanda, M. Synthesis, radio-synthesis and in vitro evaluation of terminally fluorinated derivatives of HU-210 and HU-211 as novel candidate PET tracers. *Org. Biomol. Chem.* **2017**, *15*, 2086−2096.
(57) Jiang, S.; Iliopoulos-Tsoutsouvas, C.; Tong, F.; Brust, C. A.; Keenan, C. M.; Raghav, J. G.; Hua, T.; Wu, S.; Ho, J. H.; Wu, Y.; Grim, T. W.; Zvonok, N.; Thakur, G. A.; Liu, Z. J.; Sharkey, K. A.; Bohn, L. M.; Nikas, S. P.; Makriyannis, A. Novel Functionalized Cannabinoid Receptor Probes: Development of Exceptionally Potent Agonists. *J. Med. Chem.* **2021**, *64*, 3870−3884.
(58) Bailey, W. F.; Punzalan, E. R. Convenient General Method for the Preparation of Primary Alkyllithiums by Lithium-Iodine Exchange. *J. Org. Chem.* **1990**, *55*, 5404−5406.
(59) Self-immolation of 5-chloropentyl lithium was averted by preparation at −78 °C prior to electrophile addition and optimization of *t*-BuLi equivalents. See the Supporting Information for details.
(60) Hoffmann, C.; Castro, M.; Rinken, A.; Leurs, R.; Hill, S. J.; Vischer, H. F. Ligand Residence Time at G-protein-Coupled Receptors-Why We Should Take Our Time To Study It. *Mol. Pharmacol.* **2015**, *88*, 552−560.
(61) Copeland, R. A. The drug-target residence time model: a 10-year retrospective. *Nat. Rev. Drug Discovery* **2016**, *15*, 87−95.
(62) Copeland, R. A.; Pompliano, D. L.; Meek, T. D. Drug-target residence time and its implications for lead optimization. *Nat. Rev. Drug Discovery* **2006**, *5*, 730−739.
(63) Sophocleous, A.; Landao-Bassonga, E.; Van't Hof, R. J.; Idris, A. I.; Ralston, S. H. The type 2 cannabinoid receptor regulates bone mass and ovariectomy-induced bone loss by affecting osteoblast differentiation and bone formation. *Endocrinology* **2011**, *152*, 2141−2149.
(64) Dhopeshwarkar, A.; Mackie, K. CB2 Cannabinoid receptors as a therapeutic target-what does the future hold? *Mol. Pharmacol.* **2014**, *86*, 430−437.
(65) Dhopeshwarkar, A.; Mackie, K. Functional Selectivity of CB2 Cannabinoid Receptor Ligands at a Canonical and Noncanonical Pathway. *J. Pharmacol. Exp. Ther.* **2016**, *358*, 342−351.
(66) Atwood, B. K.; Wager-Miller, J.; Haskins, C.; Straiker, A.; Mackie, K. Functional selectivity in CB(2) cannabinoid receptor signaling and regulation: implications for the therapeutic potential of CB(2) ligands. *Mol. Pharmacol.* **2012**, *81*, 250−263.
(67) *New Tools to Interrogate Endocannabinoid Signalling: From Natural Compounds to Synthetic Drugs*; Maccarrone, M., Ed.; The Royal Society of Chemistry: 2021.
(68) Scott-Dennis, M.; Rafani, F. A.; Yi, Y.; Perera, T.; Harwood, C. R.; Guba, W.; Rufer, A. C.; Grether, U.; Veprintsev, D. B.; Sykes, D. A. Development of a membrane-based Gi-CASE biosensor assay for profiling compounds at cannabinoid receptors. *Front. Pharmacol.* **2023**, *14*, 1158091.
(69) Manera, C.; Malfitano, A. M.; Parkkari, T.; Lucchesi, V.; Carpi, S.; Fogli, S.; Bertini, S.; Laezza, C.; Ligresti, A.; Saccomanni, G.; Savinainen, J. R.; Ciaglia, E.; Pisanti, S.; Gazzerro, P.; Di Marzo, V.; Nieri, P.; Macchia, M.; Bifulco, M. New quinolone- and 1,8-naphthyridine-3-carboxamides as selective CB2 receptor agonists with anticancer and immuno-modulatory activity. *Eur. J. Med. Chem.* **2015**, *97*, 10−18.
(70) Bouaboula, M.; Poinot-Chazel, C.; Marchand, J.; Canat, X.; Bourrie, B.; Rinaldi-Carmona, M.; Calandra, B.; Le Fur, G.; Casellas, P. Signaling pathway associated with stimulation of CB2 peripheral cannabinoid receptor. Involvement of both mitogen-activated protein kinase and induction of Krox-24 expression. *Eur. J. Biochem.* **1996**, *237*, 704−711.
(71) Howlett, A. C.; Abood, M. E. CB1 and CB2 Receptor Pharmacology. *Adv. Pharmacol.* **2017**, *80*, 169−206.
(72) Huffman, J. W.; Liddle, J.; Yu, S.; Aung, M. M.; Abood, M. E.; Wiley, J. L.; Martin, B. R. 3-(1',1'-Dimethylbutyl)-1-deoxy-delta8-THC and related compounds: synthesis of selective ligands for the CB2 receptor. *Biorg. Med. Chem.* **1999**, *7*, 2905−2914.
(73) Hashiesh, H. M.; Sharma, C.; Goyal, S. N.; Jha, N. K.; Ojha, S. Pharmacological Properties, Therapeutic Potential and Molecular Mechanisms of JWH133, a CB2 Receptor-Selective Agonist. *Front. Pharmacol.* **2021**, *12*, 702675.
(74) Zoratti, C.; Kipmen-Korgun, D.; Osibow, K.; Malli, R.; Graier, W. F. Anandamide initiates Ca(2+) signaling via CB2 receptor linked to phospholipase C in calf pulmonary endothelial cells. *Br. J. Pharmacol.* **2003**, *140*, 1351−1362.
(75) Juan-Pico, P.; Fuentes, E.; Bermudez-Silva, F. J.; Javier Diaz-Molina, F.; Ripoll, C.; Rodriguez de Fonseca, F.; Nadal, A. Cannabinoid receptors regulate Ca(2+) signals and insulin secretion in pancreatic beta-cell. *Cell Calcium* **2006**, *39*, 155−162.
(76) Brailoiu, G. C.; Deliu, E.; Marcu, J.; Hoffman, N. E.; Console-Bram, L.; Zhao, P.; Madesh, M.; Abood, M. E.; Brailoiu, E. Differential activation of intracellular versus plasmalemmal CB2 cannabinoid receptors. *Biochemistry* **2014**, *53*, 4990−4999.
(77) Atwood, B. K.; Lopez, J.; Wager-Miller, J.; Mackie, K.; Straiker, A. Expression of G protein-coupled receptors and related proteins in HEK293, AtT20, BV2, and N18 cell lines as revealed by microarray analysis. *BMC Genomics* **2011**, *12*, 14.
(78) Henn, A.; Lund, S.; Hedtjarn, M.; Schrattenholz, A.; Porzgen, P.; Leist, M. The suitability of BV2 cells as alternative model system for primary microglia cultures or for animal experiments examining brain inflammation. *ALTEX* **2009**, *26*, 83−94.
(79) Olajide, O. A.; Iwuanyanwu, V. U.; Adegbola, O. D.; Al-Hindawi, A. A. SARS-CoV-2 Spike Glycoprotein S1 Induces Neuroinflammation in BV-2 Microglia. *Molecular Neurobiology* **2022**, *59*, 445−458.
(80) Yao, K.; Zu, H. B. Microglial polarization: novel therapeutic mechanism against Alzheimer's disease. *Inflammopharmacology* **2020**, *28*, 95−110.
(81) Stansley, B.; Post, J.; Hensley, K. A comparative review of cell culture systems for the study of microglial biology in Alzheimer's disease. *J. Neuroinflammation* **2012**, *9*, 115.
(82) Franklin, A.; Stella, N. Arachidonylcyclopropylamide increases microglial cell migration through cannabinoid CB2 and abnormal-cannabidiol-sensitive receptors. *Eur. J. Pharmacol.* **2003**, *474*, 195−198.
(83) Han, Q. W.; Shao, Q. H.; Wang, X. T.; Ma, K. L.; Chen, N. H.; Yuan, Y. H. CB2 receptor activation inhibits the phagocytic function of microglia through activating ERK/AKT-Nurr1 signal pathways. *Acta Pharmacol. Sin.* **2022**, *43*, 2253−2266.

https://doi.org/10.1021/acscentsci.3c01461
ACS Cent. Sci. 2024, 10, 956−968

(84) Hauser, A. S.; Kooistra, A. J.; Munk, C.; Heydenreich, F. M.; Veprintsev, D. B.; Bouvier, M.; Babu, M. M.; Gloriam, D. E. GPCR activation mechanisms across classes and macro/microscales. *Nat. Struct. Mol. Biol.* **2021**, *28*, 879−888.
(85) Filipek, S. Molecular switches in GPCRs. *Curr. Opin. Struct. Biol.* **2019**, *55*, 114−120.

https://doi.org/10.1021/acscentsci.3c01461
ACS Cent. Sci. 2024, 10, 956−968